NMR Solution Structure of a Nonanucleotide Duplex with a dG Mismatch Opposite a 10*S* Adduct Derived from Trans Addition of a Deoxyadenosine N^6-Amino Group to (+)-(7*R*,8*S*,9*S*,10*R*)-7,8-Dihydroxy-9,10-epoxy-7,8,9,10-tetrahydrobenzo[a]pyrene: An Unusual *syn* Glycosidic Torsion Angle at the Modified dA[†,‡]

Herman J. C. Yeh,*[,§] Jane M. Sayer,[§] Xiaohong Liu,[§] Amanda S. Altieri,[∥] R. Andrew Byrd,[∥] Mahesh K. Lakshman,[§] Haruhiko Yagi,[§] Eric J. Schurter,[⊥] David G. Gorenstein,[⊥] and Donald M. Jerina[§]

NIDDK, The National Institutes of Health, Bethesda, Maryland 20892, Macromolecular Structure Laboratory, ABL-Basic Research Program, NCI−Frederick Cancer Research & Development Center, Frederick, Maryland 21702, and Department of Chemistry, Purdue University, West Lafayette, Indiana 47907

Received April 7, 1995; Revised Manuscript Received July 3, 1995[⊗]

ABSTRACT: A nonanucleotide, d($G_1G_2T_3C_4$[BaP]$A_5C_6G_7A_8G_9$), in which (+)-(7*R*,8*S*,9*S*, 10*R*)-7,8-dihydroxy-9,10-epoxy-7,8,9,10-tetrahydrobenzo[a]pyrene (7-hydroxyl group and epoxide oxygen are trans) is covalently bonded to the exocyclic N^6-amino group of deoxyadenosine (dA_5) through trans addition at C10 of the epoxide (to give a 10*S* adduct) has been synthesized. The solution structure of the duplex, d($G_1G_2T_3C_4$[BaP]$A_5C_6G_7A_8G_9$)·d($C_{10}T_{11}C_{12}G_{13}G_{14}G_{15}A_{16}C_{17}C_{18}$), containing a dG mismatch opposite the modified dA (designated 10*S*-[BaP]dA·dG 9-mer duplex) has been investigated using a combination of 1D and 2D (including COSY, PECOSY, TOCSY, NOESY, and indirect detection of $^1H-^{31}P$ HETCOR) NMR spectroscopies. The NMR results together with restrained molecular dynamics/energy minimization calculations show that the modified dA_5 adopts a *syn* glycosidic torsion angle whereas all other nucleotide residues adopt *anti* glycosidic torsion angles. The sugar ring of dA_5 is in the C3′-endo conformation, and the sugar rings of the other residues are in the C2′-endo conformation. The hydrocarbon attached at dA_5 orients toward the 3′ end of the modified strand (i.e., dC_6 direction) and intercalates between and parallel to bases of dG_{13} and dG_{14} of the complementary strand directly opposite dC_6 and dA_5, respectively. The edge of the hydrocarbon bearing H11 and H12 is positioned between the imino protons of dG_{13} and dG_{14} in the interior of the duplex, whereas H4 and H5 at the opposite edge are positioned near the sugar H1′ and H2″ protons of dG_{13} and facing the exterior of the duplex. The mismatched AG base pair is stabilized by $dA_{syn}-dG_{anti}$ base pairing in which the imino proton and the O^6 of dG_{14} are hydrogen bonded to N7- and the single N^6-amino proton, respectively, of the modified dA_5. The modified DNA duplex remains in a right-handed helix, which bends at the site of intercalation about 20 to 30° away from the helical axis and toward the direction of the modified strand.

Chemical modification of DNA by reactive metabolites provides the most likely mechanism for the genotoxicity, mutagenicity, and/or carcinogenicity of many xenobiotic compounds including polycyclic aromatic hydrocarbons (PAHs). Mammalian metabolism of PAHs mediated by the microsomal enzymes cytochrome P450 and epoxide hydrolase yields, among other products, diol epoxides on angular benzo rings of the hydrocarbons [reviewed in Thakker et al. (1985, 1988)]. As illustrated for benzo[a]pyrene (BaP) in Figure 1a, four optically active diol epoxides with the epoxide in the bay region of the hydrocarbon (Jerina et al., 1976; Jerina & Daly, 1976) can be metabolically formed: two enantiomers of the diastereomer in which the benzylic 7-hydroxyl group and epoxide oxygen are cis (syn diol epoxide or DE1) and two enantiomers of the diastereomer in which these groups are trans (anti or DE2). Studies both *in vivo* and *in vitro* have indicated that the major PAH adducts of DNA result from nucleophilic attack of the exocyclic N^6- and N^2-amino groups of adenine (A) and guanine (G), respectively, to open the epoxide ring of these diol epoxides at the benzylic position [reviewed in Jerina et al. (1991)]. In the case of benzo[a]pyrene (Meehan & Straub, 1979; Cheng et al., 1989), the predominant adduct formed by reaction of the most tumorigenic (Jerina et al., 1984) enantiomer, (+)-(7*R*,8*S*,9*S*,10*R*)-7,8-dihydroxy-9,10-epoxy-7,8,9,10-tetrahydrobenzo[a]pyrene [(+)-BaP DE2], with DNA *in vitro* results from trans ring opening by the exocyclic N^2-amino group of guanine. Modification at the exocyclic N^6-amino group of dA also occurs to a lesser extent, as illustrated in Figure 1b. Mutations induced by high doses of this isomer at the *HPRT* locus in Chinese hamster V79 cells are predominantly at dG; however, at lower doses, such as might result from environmental exposure to the hydrocarbon, there is a marked increase in the relative frequency of mutations at dA (Wei et al., 1991, 1993, 1994). In particular, an increase in the relative frequency in A→C

[†] This research was sponsored, in part, by the National Cancer Institute, DHHS, under contract NO1-CO-46000 with ABL (A.S.A. and R.A.B.).

[‡] The coordinates have been deposited in the Brookhaven Protein Data Bank (file name 1DXA).

[§] NIDDK, NIH.

[∥] NCI−Frederick Cancer Research & Development Center.

[⊥] Purdue University.

[⊗] Abstract published in *Advance ACS Abstracts,* September 1, 1995.

0006-2960/95/0434-13570$09.00/0

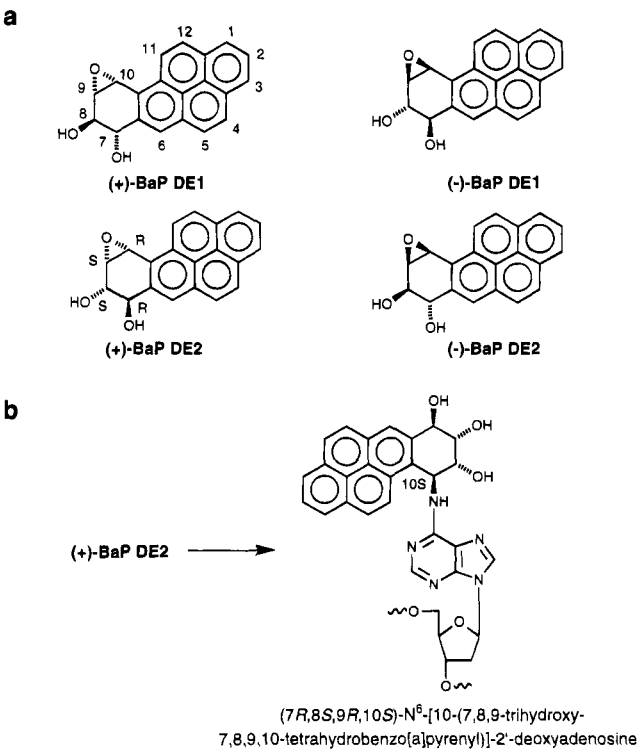

FIGURE 1: (a) Chemical structures of the four 7,8-diol-9,10-epoxide metabolites of benzo[a]pyrene and (b) the adduct derived from trans addition of the exocyclic N^6-amino group of deoxyadenosine to (+)-(7*R*,8*S*,9*S*,10*R*)-7,8-dihydroxy-9,10-epoxy-7,8,9,10-tetrahydrobenzo[a]pyrene [(+)-BaP DE2].

transversions, suggestive of a misinsertion of dG opposite the lesion site upon DNA replication, is observed at the lower doses of the diol epoxide (Wei et al., 1993, 1994). We have previously reported (Schurter et al., 1995a) that substitution of dG for dT as the complementary residue opposite the modified dA in the double-stranded oligonucleotide d(G_1G_2-T_3C_4[BaP]$A_5C_6G_7A_8G_9$)·d($C_{10}T_{11}C_{12}G_{13}G_{14}G_{15}A_{16}C_{17}C_{18}$) (derived from (+)-BaP DE2 and designated as the 10*S*-[BaP]-dA·dG 9-mer duplex) increases the thermal stability of the duplex, with an increase in T_m from 16 (complementary dT) to 27 °C (complementary dG). In the present study we report the NMR solution structure of this duplex containing dG opposite the modified dA. Of particular interest is the finding that in the present structure the modified dA adopts a *syn* conformation, which is stabilized by hydrogen bonding (Li et al., 1991) to the complementary guanine in an unusual dA_{syn}–dG_{anti} base pair.

MATERIALS AND METHODS

Sample Preparation. As previously reported (Schurter et al., 1995a), two nonanucleotides, d($G_1G_2T_3C_4$[BaP]A_5C_6-$G_7A_8G_9$), were synthesized by direct incorporation of a modified dA phosphoramidite derived from racemic BaP DE2 at the central ([BaP]A_5) position, using the approach described by Lakshman et al. (1992). These nonanucleotides were diastereomers corresponding to trans opening of the enantiomeric BaP diol epoxides (−)-(7*S*,8*R*,9*R*,10*S*)-DE2 and (+)-(7*R*,8*S*,9*S*,10*R*)-DE2 by the N^6-amino group of dA and have 10*R* and 10*S* absolute configuration, respectively, at the N-substituted benzylic carbon atom of the hydrocarbon, as a result of inversion of configuration at this carbon (cf. Figure 1b). Full details of the syntheses will be published elsewhere. The oligonucleotide with 10*S* absolute configuration of the adduct, corresponding to trans addition to the (+)-DE2 isomer, which is the subject of the present study, was >96% pure as indicated by capillary zone electrophoresis. Stoichiometry for duplex formation was determined as described (Schurter et al., 1995a) by spectrophotometric titration (362 nm) of a sample of the modified oligonucleotide with its partially complementary strand, d($C_{10}T_{11}C_{12}G_{13}G_{14}G_{15}$-$A_{16}C_{17}C_{18}$), at 5 °C in a buffer containing 12 mM Na_2HPO_4, 8 mM NaH_2PO_4, and 56 mM NaCl (to give a total ionic strength of 0.1 M) at pH 7. The sample used for the NMR studies consisted of approximately 180 A_{260} units of duplex in 500 μL of the buffer described above in D_2O (or 90% H_2O), containing 0.2 mM EDTA and a trace of sodium azide, adjusted to pH 6.8 with NaOD.

NMR Experiments. 1D, COSY, PECOSY, TOCSY, and NOESY spectra were recorded on a Varian VXR 500S (500 MHz) spectrometer at a regulated temperature of 15 °C. The 1D spectrum in H_2O was obtained using the standard BINOM pulse sequence (Hore, 1983). A NOESY spectrum (mixing time 200 ms) was also obtained using a Bruker AMX-600 (600 MHz) to improve the spectral resolution for resonance assignments. TOCSY spectra (Bax & Davis, 1985) were recorded at mixing times of 30, 50, and 80 ms. NOESY spectra were recorded at 50, 80, 120, 160, and 200 ms. The two-dimensional NMR experiments were usually carried out in the hypercomplex, phase-sensitive mode (States et al., 1982) with a 3.0 s relaxation delay between scans. Spectra were generally acquired with 1024 complex points in the t_2 dimension and 512 t_1 complex increments and were zero filled to 2K × 2K before Fourier transformation. For data processing, a Gaussian or shifted squared sine-bell weighting function was used in both dimensions. The NOESY cross peak intensities between H8 (or H6) of each base and its own sugar H1′ were used to distinguish qualitatively between *syn* (strong NOE) and *anti* (weak NOE) glycosidic torsion angles (Wüthrich, 1986).

For assignment of the exchangeable protons, NOESY (90% H_2O, mixing time 300 ms) spectra were run on a 500 MHz Varian Unity Plus spectrometer equipped with pulse shaping and *Z*-axis pulsed field gradient hardware. The experiments were run at 10 °C using the RAWSCUBA (Altieri & Byrd, 1995) NOESY pulse sequence with WATERGATE (Piotto et al., 1992) read pulse element. The experimental parameters are as follows: sw = 10 000 Hz, 1024 × 256 complex points in ω_2 and ω_1, respectively, 44 scans per increment, and STATES-TPPI (Marion et al., 1989) for quadrature detection in t_1. RAWSCUBA was run with a 10.0 ms Gaussian shaped pulse, 17 G/cm *Z*-axis gradient pulses of 5.0 ms duration, and a 60.0 ms SCUBA period (Altieri & Byrd, 1995). The WATERGATE read pulse sequence was run with 1.3 ms selective pulses centered on the water resonance and 2 G/cm *Z*-gradient pulses of 2.0 ms duration followed by 100 μs stabilization delays. An additional Z-gradient of 9 G/cm and 3.0 ms duration was used at the end of the mixing time.

The $^1H-^1H$ vicinal coupling constants (^3J) between sugar protons were analyzed from the phase-sensitive PECOSY (Müller, 1987; Bax & Lerner, 1988) spectrum, which was acquired with 2048 complex points in the t_2 dimension and 400 t_1 complex increments and zero filled to 8K × 2K before Fourier transformation.

The indirect detection $^1H-^{31}P$ HETCOR experiment was performed on a 500 MHz Varian Unity Plus spectrometer with a pulse sequence similar to that reported earlier (Sklenár et al., 1986).

Energy Minimization/Dynamics Calculations. Restrained molecular dynamics/energy minimization (rMD/rEM) calculations were performed on a Silicon Graphics Indigo XS24 R4000 workstation using software programs from Biosym Technologies, San Diego, CA. A standard B-DNA duplex with a mismatched dA-dG base pair at the center of the titled nonamer was constructed using the biopolymer module in InsightII (version 2.3). This central dA nucleotide was then modified by incorporating the BaP moiety (with *S* absolute configuration at C10) at the N^6 of dA as shown in Figure 1b. For atoms in the hydrocarbon portion of the adduct, force field parameters were adopted from equivalent AMBER atom types, and partial charges were obtained from an *ab initio* calculation on benzo[a]pyrene (Hingerty & Broyde, 1985). Calculations were done *in vacuo* with a distance-dependent dielectric constant of $4R$ and a cutoff distance of 25 Å. The restraint file (see Supporting Information) included restraints for chiral atoms, dihedral angles, and interproton NOE distances based on the NMR data. A five part continuous distance restraint penalty function (Discover program, Biosym Technologies) was used in the calculation.

$$E = \begin{cases} E_1 + (R_1 - R_{ij})F_1 & R_{ij} < R_1 \\ K_2(R_{ij} - R_2)^2 & R_1 \le R_{ij} < R_2 \\ 0 & R_2 \le R_{ij} \le R_3 \\ K_3(R_{ij} - R_3)^2 & R_3 < R_{ij} \le R_4 \\ E_4 + (R_{ij} - R_4)F_4 & R_4 < R_{ij} \end{cases} \quad (1)$$

R_{ij} is the current value of the interproton distance, R_1 and R_4 are the distances where the harmonic potential becomes linear, R_2 and R_3 are the target lower and upper bound distances, respectively, and F_1, F_4, K_2, and K_3 are force constants. The maximum value of K_2 and K_3 was set to 30 kcal mol^{-1} $Å^{-2}$, and F_1 and F_4 were set to 1000 kcal mol^{-1} $Å^{-1}$ for all restraints in the calculations. A similar function was used for dihedral restraints.

A total of 252 distance restraints (172 intranucleotide NOEs, 54 sequential NOEs, 14 B[a]P-nucleotide NOEs, and 12 intra-B[a]P NOEs) were defined. The distance range for a NOE restraint was set between 1.8 and 2.5 Å if the intensity of the the corresponding NOE cross peak was strong, between 2.5 and 3.5 Å if the cross peak was of intermediate intensity, or between 3.5 and 5.0 Å if the cross peak was weak. Backbone dihedral angles were restrained to ranges (±20° for α, β, γ, ϵ, ζ; ±30° for δ) which were centered at values adopted by a standard B-DNA (Saenger, 1984), with the exception of certain dihedral angles of the central six residues (from γ of dC_4 to δ of dC_6 of the modified strand; from γ of dG_{13} to γ of dG_{14} for the complementary strand). The glycosidic angles were restrained to a range between −170° and −90° (Wüthrich, 1986) except for the dA_5 residue. Since the NOESY spectrum in H_2O established the presence of Watson−Crick base pairings in the adducted DNA duplex, hydrogen bond restraints (2.6−3.2 Å between the donor N and acceptor O or N) were applied to all base pairs except the central dA-dG mismatch. However, a force constant of 15 kcal mol^{-1} $Å^{-2}$ was used for the hydrogen-bond restraints (distance and planar) for the two base pairs adjacent to the modified residue.

The restrained molecular dynamics (rMD) calculations were run in 9.6 ps blocks. First, the temperature was raised to 700 K from a starting temperature of 300 K over 1.6 ps without constraints. Next, the rMD calculation continued for 4 ps, in which constraints were introduced with a scaling factor of 0.001 in the first picosecond, 10 times greater in the next picosecond, etc. In the fourth picosecond, constraints were in full effect (scaling factor of 1.0). Then the temperature was reduced to 300 K over 4 ps. The coordinates derived from each rMD run were then subjected to 100 cycles of energy minimization using the steepest descents algorithm and up to 6000 iterations of minimization using the conjugate gradients algorithm. Convergence was determined by a maximum derivative below 0.01 kcal mol^{-1} $Å^{-1}$.

Structures which did not have NOE violations greater than 0.2 Å and dihedral angle violations greater than 10° in rMD/rEM calculations were used as the starting structures for iterative relaxation matrix approach (IRMA) calculations (Boelens et al., 1988, 1989). The IRMA calculation generates a list of refined NOE distance restraints from the starting structure and a typically incomplete set of NMR data (in this case, 111 well-separated NOE cross peaks), based on a full relaxation matrix calculation and experimental NOE intensities at different mixing times. The agreement between the experimental and theoretical intensities was monitored by the R factors. Several R factors, in analogy to the forms described by Gonzalez et al. (1991), are calculated after each IRMA cycle (Biosym Technologies), including linear, quadratic, and distance-like ($A_{ij}^{-1/6}$) forms. For example, the distance-like R_r factor is defined as

$$R_r = \frac{(\sum \tau_m[(A_{ij}^{cal})^{-1/6} - (A_{ij}^{exp})^{-1/6}]^2)^{1/2}}{\sum \tau_m (A_{ij}^{exp})^{-1/6}}$$

where A_{ij} is the NOE intensity of the spin pair (ij) and τ_m is the mixing time. Despite the expected variation in the magnitude of R factors among different definitions, the calculated results show similar trends for all definitions; i.e., the R factors decrease as the structure refinement progresses and usually converge within 2−3 cycles. This process was terminated when the NMR R factor failed to drop significantly over several iterations.

RESULTS

Exchangeable Proton Spectra. Expanded 1D spectra at several temperatures in the imino proton region (10−14 ppm) for the 10*S*-[BaP]dA·dG 9-mer duplex in 90% H_2O/10% D_2O buffer are shown in Figure 2. All nine imino protons are visible, and seven resonances cluster in the region between 12 and 14 ppm. The remaining two high-field resonances are assigned to the imino protons of dG_{13} (11.22 ppm) and dG_{14} (10.32 ppm) of the complementary strand. The large upfield shift for both imino protons of dG_{13} and dG_{14} can be accounted for by base pair stacking directly over and directly under the pyrene ring of the hydrocarbon bonded to dA_5. In the region of 12−14 ppm, two resonances, which show exchange broadening from 4 to 17.5 °C, are assigned to the imino protons of the terminal dG_1 (12.75 ppm) and dG_9 (13.29 ppm) of the adducted strand. The two resonances at the lowest field are assigned to the H3 imino protons of dT_3 and dT_{11}. The imino proton resonances of the remaining three dG-dC base pairs appear in the region of 12.4−12.9 ppm.

Assignments of the exchangeable imino and amino protons were made from analysis of a phase-sensitive 2D NOESY spectrum of the modified DNA duplex in 90% H_2O buffer using the RAWSCUBA pulse sequence that allows observa-

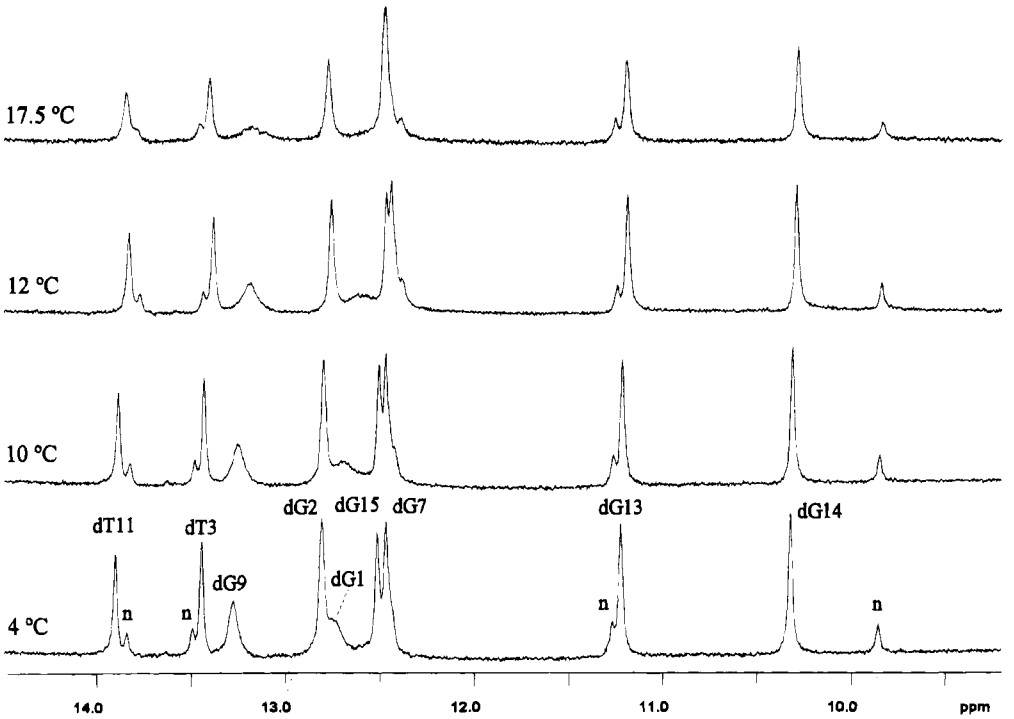

FIGURE 2: Imino proton spectra (10−14 ppm) of the 10*S*-[BaP]dA•dG 9-mer duplex in 56 mM NaCl and 20 mM phosphate, 90% H_2O, pH 6.5, at 4, 10, 12, and 17.5 °C. Resonances due to a minor conformer are designated by "n".

Table 1: Chemical Shifts (ppm, 10 °C, pH 6.5) of Labile and Selected Nonlabile Protons in Watson−Crick Base Pairs[a] in the 10*S*-[BaP]dA•dG 9-mer Duplex[b]

	imino	amino		nonlabile	
base pair	H1(dG)/H3(dT)	H4(dC)	H4(dC)	H5(dC)	H2(dA)
dG_1dC_{18}	12.75				
dG_2dC_{17}	12.81	8.12	6.57		
dT_3dA_{16}	13.46 (13.50)				7.88
dC_4dG_{15}	12.53	8.10	6.99		
[BaP]dA_5dG_{14}	10.32 (9.85)	7.20[c]	4.02[d]		7.78[e]
dC_6dG_{13}	11.22 (11.26)	8.12	7.24	6.03	
dG_7dC_{12}	12.48 (12.45)	8.42	6.87		
dA_8dT_{11}	13.93 (13.85)				7.67
dG_9dC_{10}	13.29				

[a] All in Watson−Crick base pairs except the $dA_{5(syn)}$•$dG_{14(anti)}$. [b] H1(dG), proton at the guanine position 1 in a dGdC (or dGdA) base pair; H3(dT), proton at thymine position 3 in a dTdA base pair; H4(dC) and H4(dC), hydrogen-bonded (underlined) and non-hydrogen-bonded protons of the amino group at position 4 of cytosine. The numbers in parentheses are chemical shifts for the minor isomer. [c] Amino proton of the modified dA_5. [d] Tentatively assigned to the amino protons of dG_{14}. [e] H8 of the modified dA_5.

tion of exchangeable peaks without saturation (Altieri & Byrd, 1995). In double-stranded DNA, the distance between adjacent base pairs is about 3.4 Å, and NOE cross peaks can be detected between neighboring imino protons. We have observed NOE cross peaks between seven nonterminal imino proton resonances (Figure 3). Sequential assignment (Table 1) of the nonterminal imino protons can be made by tracing through these cross peaks as previously described (Boelens et al., 1985; Hare et al., 1983). Thus, connectivity could be traced through *three* stacked base pairs (dC_6-dG_{13}, dG_7-dC_{12}, dA_8-dT_{11}) and through *four* stacked base pairs including the [BaP]dA_5-dG_{14} mismatched pair (dG_2-dC_{17}, dT_3-dA_{16}, dC_4-dG_{15}, and dA_5-dG_{14}) with a discontinuity occurring between the adjacent dC_6-dG_{13} and dA_5-dG_{14} pairs. The discontinuity between these two base pairs indicates structural perturbation occurring at this junction, resulting from the intercalation of the hydrocarbon at the modified site. No NOE cross peaks between the terminal imino protons of dG_1-dC_{18} and dG_9-dC_{10} and the protons at the adjacent base pair were detected.

The methyl protons of dT_3 and dT_{11} exhibit weak NOE cross peaks to their own imino proton and the imino proton of the adjacent stacked base pair at their flanking 3′ end. This observation permits identification of the imino protons of dT_3 (13.46 ppm) and dT_{11} (13.93 ppm). Additional NOE cross peaks involving the imino proton resonances are shown in Figure 3. We observe strong NOE cross peaks between the H3 of dT_{11} and H2 of dA_8 (7.70 ppm), and between the H3 of dT_3 and H2 of dA_{16} (7.88 ppm), establishing Watson−Crick base pairing for these dA-dT pairs. No clear inter-base-pair NOE interactions between the imino protons of dTs and the amino protons of dAs are observed. This is probably due to fast exchange and/or rotational broadening of the adenine amino resonances.

For the mismatched dA_5-dG_{14} pair, the dG imino proton (10.32 ppm) exhibits a strong NOE contact to the H8 of dA_5 (7.78 ppm). The identity of this signal as H8 rather than H2 was verified by a deuterium exchange experiment (see below), which showed that the NOE cross peak between this resonance and the imino proton resonance of dG_{14} was lost upon prolonged heating of the modified duplex in D_2O and was restored after back exchange with H_2O. We detect a very strong NOE cross peak between the dG_{14} imino proton and a proton resonating at 7.15 ppm which is tentatively assigned to the single amino proton of dA_5 (the other amino proton being replaced by the hydrocarbon).

For each dG-dC base pair, we observe strong NOE cross peaks between the imino proton of guanine and both cytosine amino protons. Identification of the amino protons was based on the observation of a *very* strong NOE cross peak between the two protons of a single amino group (1.7 Å internuclear distance) and of NOE interactions between both these amino protons and the H5 (and H6) of cytosine. The latter protons are readily identified from the COSY spectrum in D_2O. Since

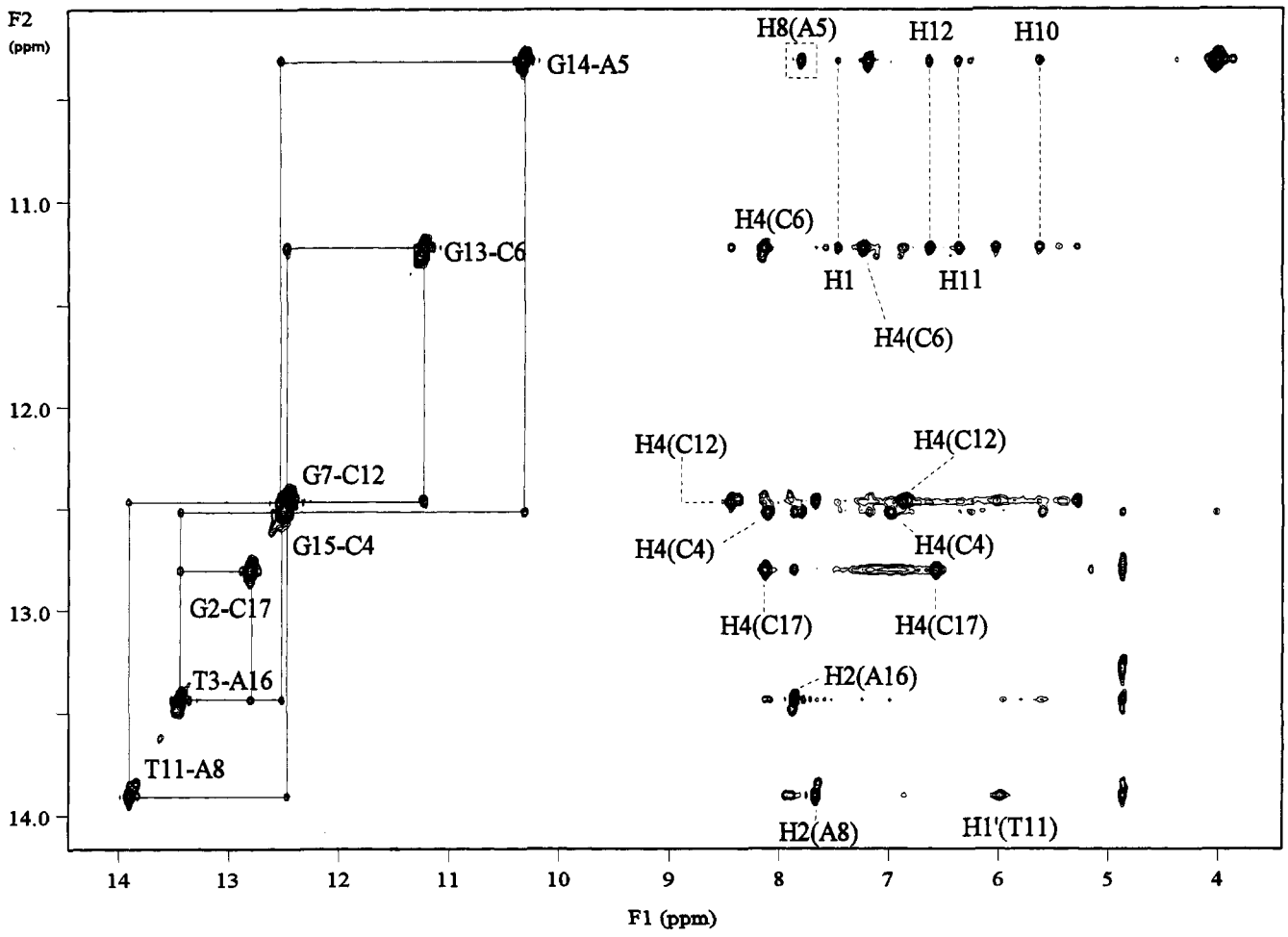

FIGURE 3: Expanded NOESY contour plots (mixing time 300 ms) of the 10*S*-[BaP]dA·dG 9-mer duplex in 56 mM NaCl and 20 mM phosphate, 90% H_2O, pH 6.5, at 10 °C. NOE cross peak connectivities between the imino protons (10−14 ppm) and the amino, base, and hydrocarbon (4−9 ppm) protons are shown. The absence of an NOE cross peak between the imino protons of the adjacent dG_{13} and dG_{14} and the presence of NOE cross peaks between the imino protons of dG_{13} as well as dG_{14} and the hydrocarbon protons clearly indicate that the pyrene moiety is positioned between the dG_{13} and dG_{14} residues. The cross peak between the imino proton of dG_{14} and the H8 of dA_5 (boxed) disappeared when the duplex was heated in D_2O at 65 °C to exchange the H8 protons of dA and dG with deuterium. This observation confirms the *syn* conformation for the glycosidic bond of the dA_5 residue.

the NOE contact from the imino proton of dG to the low-field dC amino proton in each dG-dC pair is stronger than that to the higher-field amino proton, it is concluded that the low-field cytosine amino proton is the one involved in Watson−Crick hydrogen bonding. No NOE interaction between the imino and amino protons of the same guanine was detected in any of the dG-dC base pairs, probably due to fast exchange and/or rotational broadening of the amino proton resonances of dG.

Observed NOE cross peaks between the imino protons of both dG_{13} and dG_{14} and the H1, H10, H11, and H12 of the hydrocarbon (Figure 3) indicate the proximity of both these imino protons to the hydrocarbon as a result of its intercalation into the DNA. These two imino proton resonances are also shifted upfield relative to the imino protons of the other dG-dC pairs, because of their stacking directly above or below the pyrene moiety. Intercalation of the pyrene moiety between the adjacent dG_{13} and dG_{14} is also consistent with the observed interruption (see above) of the NOE connectivity pathway between the imino protons of these adjacent bases.

The 1D spectra (Figure 2) also reveal the presence of a minor conformer (~17%, labeled as n) which is in slow exchange with the major conformer on the NMR time scale. The presence of the minor conformer is discernible in the regions of imino and hydrocarbon proton resonances, particularly the imino proton of dG_{14} (and other imino protons) and H4, H5, H11, and H12 of the pyrenyl moiety (Table 1). However, nonexchangeable proton resonances in regions away from the modified site of the minor conformer are unresolvable from the corresponding resonances of the major conformer (due to severe signal overlap), suggesting a high degree of structural similarity between the two conformers in these regions. No attempt was made to assign the resonances or to determine the structure of the minor conformer, and no correction in the rMD/rEM calculations was applied for overlapping cross peaks due to the minor conformer.

Nonexchangeable DNA Proton Spectra. The sequential connectivities along each strand of the 10*S*-[BaP]dA·dG 9-mer duplex were established by tracing through NOE cross peaks between the base protons (H8/H6) and their own and 5′-flanking sugar H1′ (and also H2′−H4′) protons. Expanded NOESY (mixing time, 200 ms) contour plots in the region for the base protons (6.8−8.8 ppm) and the sugar H1′ protons (4.6−6.3 ppm) together with the connectivity pathways (indicated by lines) for the modified and complementary strands are shown, respectively, in Figure 4, panels a and b. Notably, two NOE cross peaks are missing or extremely weak along the base to sugar H1′ sequential connectivity

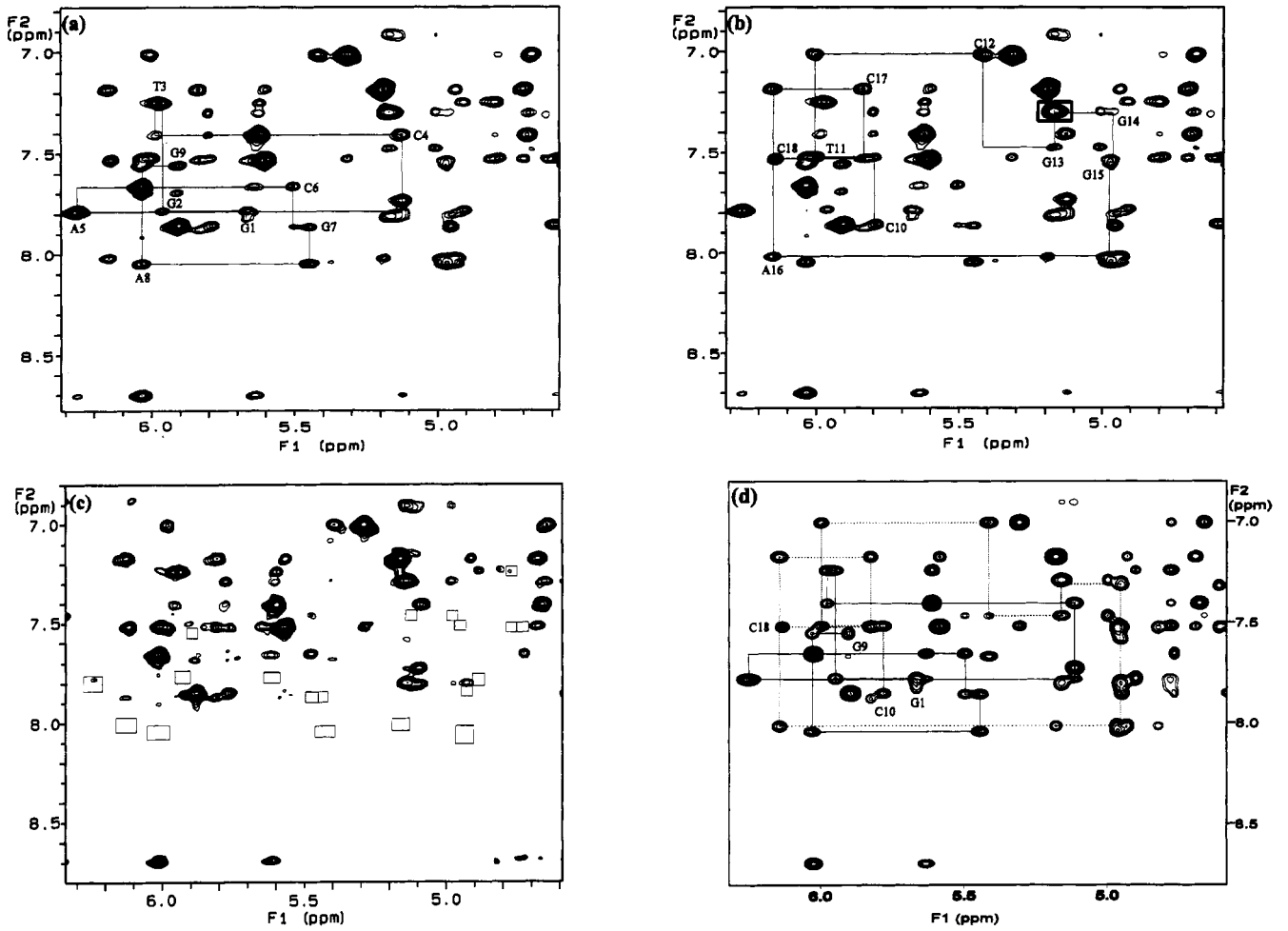

FIGURE 4: Expanded NOESY contour plots (mixing time 200 ms) of the 10*S*-[BaP]dA·dG 9-mer duplex in D_2O containing 56 mM NaCl and 20 mM phosphate, pH 6.8, at 15 °C. (a) The sequential NOE connectivity pathway between the base protons (6.8−8.8 ppm) and the sugar H1′ (4.5−6.5 ppm) of the modified strand. (b) The NOESY connectivity pathway in the same region as panel a but for the complementary strand. The cross peak between the hydrocarbon H4 of the adduct and H1′(dG_{13}) is boxed. (c) Expanded NOESY spectrum in the same region as panel a (or panel b) after heating the sample to 65 °C in D_2O for 25 h. The boxed regions identify cross peaks that vanished after deuterium exchange. (d) Expanded simulated NOESY spectrum (mixing time 200 ms) from the final refined structure.

path of the modified strand (Figure 4a). These are cross peaks from the H1′ (5.15 ppm) of dC_4 to the H8 (7.79 ppm) of the modified dA_5 and from the H1′ (6.25 ppm) of the modified dA_5 to the H6 (7.66 ppm) of dC_6. We also note missing or very weak cross peaks in the base proton to sugar H1′ sequential path at dC_{12}-dG_{13} and dG_{13}-dG_{14} for the complementary strand (Figure 4b). These observations are consistent with the NOESY data in 90% H_2O, which also show discontinuity between the imino protons of dG_{13} and dG_{14} (Figure 3). These breaks in connectivity paths indicate local distortions resulting from the covalent bonding of the diol epoxide at the dA_5 site. Sequential connectivities between the base protons and the sugar H2′ and H2″ (and H3′ and H4′) were also established by tracing through NOE cross peaks in other regions of the NOESY spectrum.

We also detected sequential NOE interactions between H5 of the cytosines and the base and sugar protons of the residue in the position 5′ to them. These include H5 of dC_4 to H2′, H2″, H3′, H6, and Me of dT_3, H5 of dC_6 to H3′ of dA_5, H5 of dC_{12} to H1′, H2′, H2″, H3′, H6, and Me of dT_{11}, H5 of dC_{17} to H1′ and H8 of dA_{16}, and H5 of dC_{18} to H1′, H2′, H2″, H3′, H5, and H6 of dC_{17}. NOE interactions from the Me of dT_3 to H1′, H3′, and H8 of dG_2, and Me of dT_{11} to H1′, H3′, H5, and H6 of dC_{10} are also detected. A very weak NOE cross peak between the H1′ (5.1 ppm) of dC_4 and the H2 (8.69 ppm) of the modified dA_5 is also noted. These sequential NOE patterns are consistent with the preservation of a B-DNA conformation in the modified DNA duplex. The resonance assignments of the sugar protons derived from the through-space connectivities (NOESY data) were internally consistent with assignments deduced from analysis of the through-bond COSY and TOCSY spectra. The complete chemical shift assignments for the nonexchangeable base and sugar protons (except H5′ and H5″ due to severe overlap of resonances) for the entire adduct duplex are listed in Table 2.

A particularly striking spectral feature of the present modified DNA duplex is the very strong NOE cross peak between H8 (7.79 ppm) of the modified dA_5 and its sugar H1′ (6.25 ppm), whose intensity (50 ms mixing time) is almost as large as that of the H5-H6 of deoxycytidine. This strong intraresidue NOE interaction between H8 and H1′ is indicative of a *syn* glycosidic torsion angle (Wüthrich, 1986) at the modified dA_5. This assigned H8 resonance (7.79 ppm) of dA_5 in the present structure appears at ~0.9 ppm higher field than H2 (8.69 ppm) which is the most downfield signal among nonexchangeable protons. The chemical shifts of these two protons are reversed when compared with those of the modified adenine in other BaP adducted DNA duplexes that have been reported (Schurter et al., 1995a,b). Since the final structural analysis depends upon the correct assignment of the H2 and H8 of dA_5, unambiguous assign-

Table 2: Chemical Shift Assignments (in ppm) for Nucleotide Protons (except H5′ and H5″) of the 10*S*-[BaP]dA·dG 9-mer Duplex

	H1′	H2′	H2″	H3′	H4′	H6/H8	H5	H2	Me
dG_1	5.66	2.54	2.65	4.78	4.26	7.82			
dG_2	5.95	2.58	2.72	4.90	4.34	7.78			
dT_3	5.96	1.98	2.29	4.79	4.16	7.24			1.31
dC_4	5.11	1.74	0.91	4.68	4.05	7.40	5.61		
[BaP]dA_5	6.25	2.59	2.75	5.62	4.29	7.79		8.69	
dC_6	5.50	2.05	2.26	4.73	4.08	7.66	6.03		
dG_7	5.44	2.64	2.67	4.94	4.06	7.86			
dA_8	6.03	2.59	2.83	4.96	4.34	8.04		7.70	
dG_9	5.90	2.30	2.17	4.53	4.06	7.55			
dC_{10}	5.78	2.17	2.50	4.57	4.03	7.85	5.90		
dT_{11}	6.00	2.05	2.38	4.77	4.16	7.51			1.59
dC_{12}	5.40	1.46	1.90	4.66	3.88	7.01	5.30		
dG_{13}	5.16	2.57	2.88	5.00	4.18	7.47			
dG_{14}	4.96	2.06	2.42	4.62	4.00	7.28			
dG_{15}	4.98	2.40	2.45	4.83	4.15	7.54			
dA_{16}	6.14	2.57	2.79	4.92	4.37	8.01		7.88	
dC_{17}	5.82	1.94	2.32	4.69	4.07	7.18	5.18		
dC_{18}	6.14	2.17	2.18	4.46	3.95	7.52	5.59		

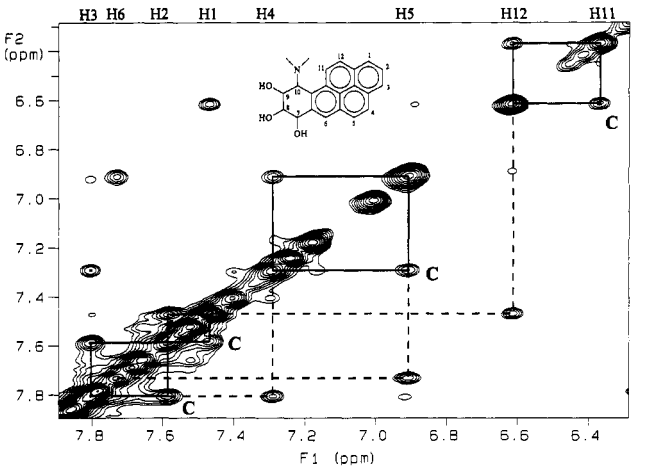

FIGURE 5: Expanded NOESY contour plot in the aromatic hydrocarbon region (6.3−8.0 ppm). Cross peaks labeled with "c" are also detected in the COSY spectrum. Assignments of the aromatic protons are indicated at the top of the plot.

ment for these protons is critical. Given the absence of scalar couplings that can be used to distinguish between these two protons and the ambiguity in interpreting through-space NOE connectivities (because assignments based on such connectivities depend on assumptions about the orientation of the base), we chose to determine the assignment unambiguously by deuterium exchange. It is expected that H8 should exchange faster than H2 with solvent deuterium (Bullock & Jardetzky, 1964; Tomasz et al., 1972). Upon heating of the sample in D_2O for 25 h at 65 °C, >85% of the intensity of the resonance at 7.79 ppm was lost, whereas no change was observed for the signal at 8.69 ppm. The original spectrum was restored when back exchange with H_2O was performed. The NOESY spectrum of the 10*S*-[BaP]dA·dG 9-mer duplex after deuterium exchange (Figure 4c) lacks the cross peak between H8 (7.79 ppm) and H1′ (6.25 ppm) of the adducted residue (dA_5) as well as all other cross peaks associated with the purine H8s of dA and dG. In contrast, in the 10*R*-[BaP]-dA·dG 9-mer duplex, the low-field resonance at 8.67 ppm rather than that at 7.69 ppm underwent exchange with solvent deuterium under similar conditions (Schurter et al., 1995a), indicating that the chemical shifts for these two protons are reversed in these 9-mer duplexes. A similar reversal of the chemical shifts corresponding to H8 (7.95 ppm) and H2 (8.81 ppm) has been observed in a nonanucleotide duplex containing a modified 1,N^6-ethenodeoxyadenosine residue that also has a *syn* glycosidic torsion angle (de los Santos et al., 1991).

We also observed a moderate downfield shift (~0.6 ppm) for the H3′ of dA_5 in the 10*S*-[BaP]dA·dG 9-mer duplex. This is consistent with a structure in which this sugar proton lies in the plane of the purine base of dA_5. There is a large upfield shift (to 0.92 ppm) for the H2″ of dC_4, which stacks directly over the base of dA_5.

Deoxyribose Conformation. Vicinal coupling constants (^3J) between sugar protons provide a measure of sugar conformation, which can be described as an equilibrium mixture of rapidly interconverting C2′-endo (S-state) and C3′-endo (N-state) puckers. The predominant conformation of the deoxyribose rings of DNA duplexes can be qualitatively determined from the magnitudes of $\Sigma 1'$ (sum of $J_{1'-2'}$ and $J_{1'-2''}$), $\Sigma 2'$ (sum of $J_{1'-2'}$, $J_{2'-2''}$, and $J_{2'-3'}$), and $\Sigma 2''$ (sum of $J_{1'-2''}$, $J_{2'-2''}$, and $J_{2''-3'}$). For $\Sigma 1' > 13.5$ Hz, $\Sigma 2' > 28.0$ Hz, and $\Sigma 2'' < 23.5$ Hz, the conformation is predominantly (>50%) in the S-state (Rinkel & Altona, 1987). The value of $\Sigma 2''$ is mainly influenced by the relative N-state and S-state populations and is an excellent indicator for determining the fraction in the S-state, p_s, according to the equation $p_s = (31.5 - \Sigma 2'')/10.9$ (Rinkel & Altona, 1987). Values of $\Sigma 1'$, $\Sigma 2'$, and $\Sigma 2''$ measured from the outer peak-to-peak separation of identifiable cross peaks in the t_2 (F_2) dimension of a PECOSY spectrum (Figure S1) are in the range 13.5−16.1, 25.0−31.0, and 22.8−25.0 Hz, respectively, except for the terminal dC_{10} ($\Sigma 1' = 11.6$ Hz, $\Sigma 2' = 27.4$ Hz, and $\Sigma 2'' = 28.6$ Hz) and the modified dA_5 ($\Sigma 1' = 11.3$ Hz, $\Sigma 2' = 25.4$ Hz, and $\Sigma 2'' = 31.7$ Hz). These results indicate that the deoxyribose ring conformation of the 10*S*-[BaP]dA·dG 9-mer duplex is predominantly in the S-state (C2′-endo) for every residue with the exception of dC_{10} (p_s 27%) and the modified dA_5 (p_s <5%) which are predominantly in the N-state (C3′-endo) conformation. The predominant N-state conformation for the sugar of dA_5 determined by the scalar coupling constants is consistent with the structures derived independently from the rMD/rEM/IRMA calculations which showed a δ torsion angle of 65−75°.

Hydrocarbon Proton Spectra. Assignment of hydrocarbon ring protons for the 10*S*-[BaP]dA·dG 9-mer duplex is made from analyses of the COSY and NOESY spectra. The COSY spectrum established through-bond connectivities for three-spin (H1 7.47 ppm; H2 7.58 ppm; H3 7.80 ppm), two-spin (H4 7.29 ppm; H5 6.90 ppm; and H11 6.37 ppm; H12 6.61 ppm) and a single-spin (H6 7.72 ppm) systems in the aromatic region, and a four-spin system (H7 5.12 ppm; H8 3.88 ppm; H9 4.26 ppm; H10 5.63 ppm) for the tetrahydro benzo ring derived from the hydrocarbon. The connectivities within these spin systems are then established from the NOESY spectrum (Figure 5). This includes connectivities from H1 to H12, H3 to H4, H5 to H6 within the aromatic rings, and H6 to H7, and H10 to H11 between the tetrahydro benzo and aromatic rings. Assignments of these ring protons are listed in Table 3.

The through-bond cross peaks involving benzo-ring methine protons of the hydrocarbon are very weak due to small J couplings, with the exception of the cross peak between H7 and H8 which showed J coupling of 10.5 Hz. This is consistent with a distorted half-chair conformation of the nonaromatic ring in which the H7 and H8 protons adopt pseudodiaxial orientations whereas the H9 and H10 protons

Table 3: Chemical Shift Assignments (in ppm) for Protons of the Hydrocarbon Moiety in the 10*S*-[BaP]dA•dG 9-mer Duplex[a]

proton	chemical shift (ppm)	proton	chemical shift (ppm)
H1	7.47 (7.57)	H7	5.12 (not assigned)
H2	7.58 (7.62)	H8	3.88 (not assigned)
H3	7.80 (7.85)	H9	4.26 (not assigned)
H4	7.29 (7.15)	H10	5.63 (not assigned)
H5	6.90 (6.93)	H11	6.37 (6.58)
H6	7.72 (7.82)	H12	6.61 (6.90)

[a] Numbers in parentheses are for the minor conformer.

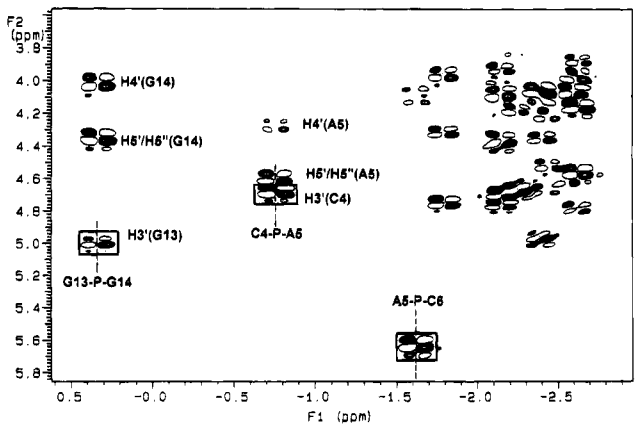

FIGURE 6: Proton-detected $^{31}P-^{1}H$ heteronuclear correlation spectrum (Varian Unity-plus) of the 10*S*-[BaP]dA•dG 9-mer duplex in D_2O containing 56 mM NaCl and 20 mM phosphate, pH 6.8, at 10 °C. The inorganic phosphate from the buffer is used as ^{31}P chemical shift reference (0.0 ppm). The resonances at 0.33, −0.76, and −1.62 ppm are assigned, respectively, to the phosphorus at the 5′ end of dG_{14}, dA_5, and dC_6. The correlation cross peaks between phosphorus and the H3′ proton of the sugar toward the 5′ end are boxed. The very strong cross peaks between both H4′ and H5′ (or H5″) of dG_{13} and P of dG_{14} indicate unusual α and β torsional angles for the dG_{13}-P-dG_{14} phosphate.

adopt pseudodiequatorial orientations. This conformation is similar to that observed for the adduct in the 10*R*-[BaP]-dA•dG 9-mer duplex derived from the enantiomeric (−)-BaP DE2 (Schurter et al., 1995a) as well as for acetylated nucleoside adducts of several polycyclic aromatic hydrocarbon diol epoxides in acetone (Cheng et al., 1989; Jerina et al., 1991).

Hydrocarbon to DNA NOEs. A total of 25 NOE cross peaks between the protons of the hydrocarbon moiety and those of the nucleic acid have been identified for the 10*S*-[BaP]dA•dG 9-mer duplex. These include eight cross peaks from the NOESY spectrum in H_2O between H1, H10, H11, and H12 of the pyrenyl residue and the hydrogen-bonded imino protons of dG_{13} and dG_{14} in the interior of the duplex, and 17 cross peaks from the NOESY spectrum in D_2O between protons at the opposite edge of the pyrene ring system (H3, H4, H5, and H6) and sugar/base protons of dC_4, dA_5, dC_6, dG_{13}, and dG_{14}.

Phosphorus Spectra. Assignments of the phosphorus resonances were made from an analysis of a proton−phosphorus heteronuclear correlation spectrum of the 10*S*-[BaP]dA•dG 9-mer duplex in 20 mM phosphate buffered D_2O (pH 7.0) at 10 °C (Figure 6). In DNA each diester phosphorus resonance correlates with the H3′ proton of the sugar on the 5′ side (three-bond H−P coupling), and the H4′ (four-bond H−P coupling) and H5′ (three-bond H−P coupling) protons on 3′ side along the chain. The phosphorus resonances can be assigned on the basis of the known sugar H3′ and H4′ proton assignments. Partial assignment of the ^{31}P resonances for the 10*S*-[BaP]dA•dG 9-mer duplex is indicated in Figure 6. The spectrum exhibits two resonances which are shifted significantly downfield from the spectral region for typical backbone phosphodiesters (−2 to −3 ppm). The most downfield-shifted phosphorus at 0.33 ppm is assigned to the phosphorus between the dG_{13} and dG_{14} of the complementary strand, while the next most downfield-shifted at −0.76 ppm is assigned to the phosphorus between the dC_4 and the modified dA_5 of the adducted strand. The downfield shifts for these ^{31}P resonances can be accounted by unusual torsion angles for the phosphate backbone in this region (Gorenstein, 1994). In addition, the relative intensities of the H3′−P, H4′−P, and H5′/H5″−P cross peaks are rather unusual for the farthest downfield-shifted ^{31}P resonance (0.33 ppm). This indicates unusual torsional angles for α, β, ϵ, and ζ (Gorenstein, 1994). The resonance at −1.62 ppm which correlates with the H3′ (5.63 ppm) of dA_5 is assigned to the phosphorus between the dA_5 and dC_6.

Energy Minimization and Solution Structure. Although the NOE data of the 10*S*-[BaP]dA•dG 9-mer duplex strongly suggested hydrocarbon intercalation and the presence of a *syn* torsion angle at the modified dA, our computational strategy was to use starting structures that are different at the modified site. Two starting structures, both with *anti* glycosidic torsion angle at the modified dA and with the hydrocarbon either positioned outside or intercalated in the interior of the duplex, were employed in the rMD/rEM calculations. Regardless of the starting structure, the computed structures that converged with ≤0.2 Å for NOE violations and ≤10° for dihedral angle violations, as well as the lower total energies, were those in which the hydrocarbon was oriented toward the 3′-side of the modified adenine and sandwiched between dG_{13} and dG_{14} of the complementary strand. Moreover, these structures all showed *syn* glycosidic torsion angles ranging from 25° to 90° and a C3′-endo (N-state) sugar pucker conformation for the modified dA_5 residue. The maximum RMS deviation from the average of these 13 best fit structures was 1.2 Å. Many of these best fit rMD/energy minimized structures were subjected to further IRMA calculations over 111 well-seperated NOE cross peaks. After IRMA calculations for each structure, the values of R_1, defined as $(\sum|A^{exp} - A^{cal}|/\sum A^{exp})$, were about 0.44 for all cross peaks and 0.56 for interresidue cross peaks. The values of R_r (defined in the Materials and Methods) were 0.006 for all cross peaks and 0.016 for interresidue cross peaks. Figure 7 shows the superpositions of five IRMA refined structures. For these five structures, the maximum RMSD from the average was about 0.5 Å. These refined structures are not much different from the corresponding input structures. However, improvements are observed in the δ and χ angles for the dA_5 residue. The values for the χ angle of dA_5 are from 26° to 60°. The values for the δ angle are from 65° to 75°. These structures retain the B form of a right-handed DNA duplex. The pyrenyl moiety is positioned between dA_5 and dC_6 and intercalates between bases of dG_{14} and dG_{13} in the complementary strand. The edge containing H11 and H12 of the pyrene ring system is located in the interior of the helix, whereas the opposite edge containing H4 and H5 lies in the major groove between dG_{13} and dG_{14}.

NOE data in H_2O were not included in the rMD/rEM/IRMA calculations to avoid errors due to possible intensity distortions arising from the long mixing time and exchange with water. Nevertheless, distances between the exchange-

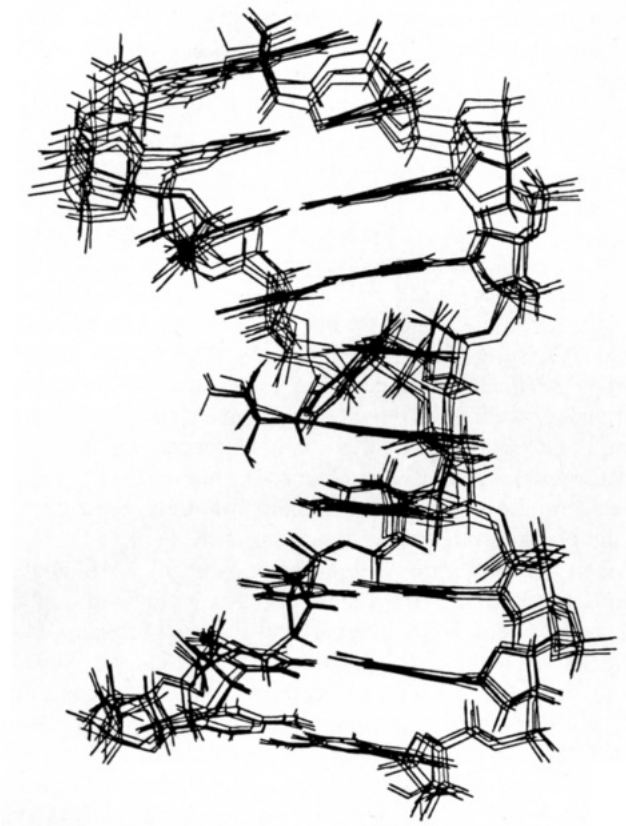

FIGURE 7: Superposition of five refined structures of the 10*S*-[BaP]-dA•dG 9-mer duplex. The 5′-end of the modified strand is at the top.

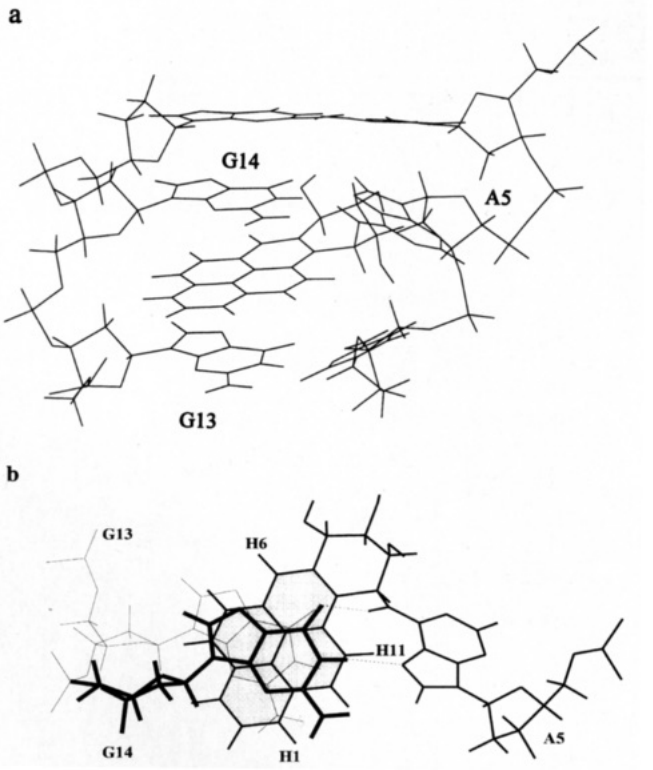

FIGURE 8: Refined structure of the d($C_4A_5C_6$)-d($G_{13}G_{14}G_{15}$) segment of the 10*S*-[BaP]dA•dG 9-mer duplex. (a) View looking into the major groove and normal to the helical axis. (b) View looking along the helical axis from the 5′- to 3′-end of the modified strand (only segment G_{13}-A_5-G_{14} is shown).

able base protons were estimated independently from this NOESY spectrum (using 1.7 Å for the geminal amino protons of cytosine as a reference). The estimated distances were about 15−30% shorter than those measured from refined structures derived exclusively from NOEs of non-exchangeable protons.

Comparison of Simulated and Experimental NOESY Spectra. One of the the refined structures was used to simulate the NOESY spectrum at the 200 ms mixing time using the BACKCAL program (Biosym Technologies). An expanded simulated NOESY plot is shown in Figure 4d. The simulation duplicated the strong NOE between H8 and H1′ of dA_5 and the same breaks between dA_5 and dC_6 and between dG_{13} and dG_{14} as in the experimental NOESY spectra (Figure 4, panel a or b). The simulation also reproduced NOEs between the DNA backbone sugars (dC_4, dA_5, dC_6, dG_{13}, and dG_{14}) and the hydrocarbon moiety.

DISCUSSION

The oligonucleotide described in the present study (10*S*-[BaP]dA•dG 9-mer duplex) has the exocyclic amino group of the central dA_5 modified by trans addition to (+)-BaP DE2. We have recently described (Schurter et al., 1995a) the structure of a similar oligonucleotide (10*R*-[BaP]dA•dG 9-mer duplex) in which the central dA_5 is modified by the enantiomeric diol epoxide, (−)-BaP DE2. Thus, the two oligonucleotides differ in that they have opposite absolute configurations at the N-substituted benzylic C10 carbon atom of the adduct as well as at the remaining three positions on the saturated benzo ring. For the present (+)-DE2 adducted 10*S*-nonamer, we observed that the thermal stability (T_m = 27 °C) of the duplex containing a dG residue opposite the adducted dA was substantially higher than that of the duplex containing the normal dT opposite dA in the complementary strand (T_m = 16 °C). However, for the previously reported 10*R*-nonamer containing a (−)-DE2 adduct, T_m values were essentially identical regardless of whether dT or dG was opposite the modified base. Comparison of the NMR solution structures of the two nonamer duplexes derived from these enantiomeric diol epoxides provides insight into the differential effects of a mismatched base opposite the hydrocarbon lesion site.

Both the present 10*S*-[BaP]dA•dG 9-mer duplex and the previously described 10*R*-[BaP]dA•dG 9-mer duplex (Schurter et al., 1995a) preserve a right-handed B-DNA type structure, except in the immediate vicinity of the modified site. Furthermore, the hydrocarbon is intercalated into the DNA helix in both structures. In the present 10*S*-[BaP]-dA•dG 9-mer duplex, the hydrocarbon orients toward the 3′-side of the modified adenine base and lies between the guanine bases of dG_{13} and dG_{14} in the complementary strand. As shown in Figure 8, the edge of the hydrocarbon containing H11 and H12 is located between the imino protons of dG_{13} and dG_{14} in the interior of the duplex, and H4 and H5 on the opposite edge are positioned toward the backbone near the sugar protons (H1′, H2′, and H2″) of dG_{13}. This orientation contrasts with that observed in the previously reported structure for the 10*R*-[BaP]dA•dG 9-mer duplex (Schurter et al., 1995a), in which the pyrene moiety intercalates on the opposite (5′) side of the modified adenine base. The same effect of chirality on the orientation of the hydrocarbon is observed in the solution conformations of three other oligonucleotides derived from trans addition of the N^6-amino group of a dA residue to the benzylic position of bay-region diol epoxides. These are an undecanucleotide duplex containing a 10*R*-[BaP]dA adduct derived from (−)-BaP DE1 (isomer with the benzylic hydroxyl and epoxide

groups cis) (Schurter et al., 1995b) and two undecanucleotide duplexes of different sequence that contain dA adducts derived from benzo[c]phenanthrene (4*S*,3*R*)-diol (2*R*,1*S*)-epoxide-2 (10*R*-[BcPh]dA adduct; Cosman et al., 1993b) and from its enantiomer, benzo[c]phenanthrene (4*R*,3*S*)-diol (2*S*,1*R*)-epoxide-2 (10*S*-[BcPh]dA adduct; Cosman et al., 1995). In all three of these duplexes, the normal dT complement is located opposite the modified dA. In the BaP and BcPh modified oligomers in which the absolute configuration at the N-substituted benzylic carbon atom is *R*, the aromatic portion of the hydrocarbon intercalates into the DNA with an orientation toward the 5′ side of the adducted dA (Schurter et al., 1995b; Cosman et al., 1993b). Conversely, in the BcPh modified oligomer with *S* absolute configuration (Cosman et al., 1995), the hydrocarbon intercalates toward the 3′ end. On the basis of the five dA adducted oligonucleotides whose NMR structures have been solved, a tentative generalization can be made that the aromatic portion of the hydrocarbon in an adducted dA residue with *R* absolute configuration at the site of attachment to the amino group of dA will orient toward the 5′ side of the modified adenine, whereas the aromatic moiety will orient in the opposite direction (i.e., 3′ end), when the absolute configuration at the substitution site is *S*.

To date, the oligonucleotides containing dA adducts whose NMR structures have been solved are all characterized by intercalation of the hydrocarbon into the DNA helix. These structures contrast with those for oligonucleotides modified at N^2 of dG residues by trans addition to BaP diol epoxides. In the presence of the normal complement, dC, the hydrocarbon moiety of dG adducts derived from trans opening of both (+)- and (−)-BaP DE2 lies in the minor groove of the DNA helix (Cosman et al., 1992; de los Santos et al., 1992). In these trans dG adducts, the orientation of the hydrocarbon relative to the DNA strand to which it is attached also depends upon the chirality at the attachment site but is opposite in direction to that observed for the intercalated trans dA adducts. Thus, in an oligonucleotide duplex containing a 10*S* dG adduct from (+)-BaP DE2, the hydrocarbon is oriented toward the 5′ end of the strand to which it is attached (Cosman et al., 1992), whereas in an oligonucleotide of the same sequence containing the 10*R* dG adduct from the enantiomeric (−)-BaP DE2, the hydrocarbon is oriented toward the 3′ end of the modified strand (de los Santos et al., 1992).

When a dG adduct is derived from cis rather than trans opening of the epoxide ring of (+)-BaP DE2 (Cosman et al., 1993a), or when the adducted strand is paired with a complementary strand with one residue deleted opposite the modified base (Cosman et al., 1994a,b), intercalation of the hydrocarbon is observed. Although NMR data are not available to assess the effect of *base pair mismatches* with modified dG residues, UV spectroscopic evidence suggests that intercalation of the hydrocarbon occurs in several duplexes with mismatches opposite dG adducts (Ya et al., 1994).

The most striking differences between the present adducted nonamer and its counterpart with the opposite absolute configuration at the site of attachment of the hydrocarbon to dA_5 involve the conformation around the glycosidic bond of the modified dA_5 and the orientation of the opposing dG. In the 10*R*-[BaP]dA·dG 9-mer duplex (Schurter et al., 1995a), the modified dA retains a normal *anti* conformation and the guanine base of dG_{14} is pushed out into the major groove leaving a space between dG_{13} and dG_{15} into which the hydrocarbon inserts. In contrast, in the present 10*S*-[BaP]-dA·dG 9-mer duplex, the modified dA_5 assumes a *syn* glycosidic torsion angle (see Figure 8), and the opposing dG_{14} remains stacked in the DNA helix and hydrogen bonded to dA_5. The *syn* glycosidic torsion angle of the modified dA_5 is supported by extensive NMR evidence: (i) There is a *very* strong NOE cross peak between the H8 of dA_5 and its own sugar H1′, which is comparable in intensity to the NOE between H5 and H6 of dC. (ii) There is also a strong NOE cross peak between H2 of the base and H2′ and H3′ of the sugar in this residue. (iii) No NOEs were detected between H8 of the modified dA_5 and the sugar H1′, H2′, H2″, and H3′ of dC_4 in the 5′ position to this residue, as would be expected for a dA residue in the normal *anti* conformation. (iv) The unusual downfield shift for the H3′ resonance (5.62 ppm) is consistent with an in-plane ring current effect by the adenine ring in a *syn* dA. (v) Further evidence for a *syn* rather than *anti* glycosidic torsion angle at the modified dA_5 comes from a strong interstrand NOE interaction from the imino proton of dG_{14} to the H8 (rather than H2) of dA_5 that can be detected only when the dA-dG mispair exists in a dA_{syn}−dG_{anti}-type hydrogen bonding (Scheme 1) in which the imino proton and the O^6 of dG_{14} are hydrogen bonded to the N^7- and the single N^6-amino proton, respectively, of the modified dA_5. The intercalated BaP wedges apart the guanine bases G_{13} and G_{14} from 3.3 to 6.7 Å, which results in the modified base twisting toward the base of dG_{14} and forming a nonplanar dA_{syn}−dG_{anti} base pair. The distances from the imino proton of dG_{14} to H8 (3.50 Å) and N^7 (2.07 Å) of dA_5, and from O^6 of dG_{14} to the N^6-amino proton of dA_5, measured from the refined structure (Figure 8) are consistent with this conformation. The intercalation and twisting by the BaP adducted dA also result in bending of the helix at the modified site by about 20−30° (Figure 7).

The conformation of an A-G mismatch in unmodified DNA (Scheme 1) depends strongly upon variables such as pH (Gao & Patel, 1988; Leonard et al., 1990) and sequence context (Brown et al., 1990). Conformations of the A_{anti}−G_{anti} and A_{anti}−G_{syn} base pairs in different DNA sequences have been established by solution NMR (Gao & Patel, 1988; Li et al., 1991; Chou et al., 1992a,b), and the existence of an A_{syn}−G_{anti} base pair has been documented in X-ray studies (Hunter et al., 1986; Webster et al., 1990). Our observation of an A_{syn}−G_{anti} conformation in the present 10*S*-[BaP]dA·dG 9-mer duplex and an A_{anti} that is not base paired with the opposing G in the previous 10*R* counterpart reflect the conformational unpredictability for an A−G mismatch in DNA duplexes modified with BaP diol epoxides.

In DNA, the overall helical twist of the duplex is influenced by the backbone conformation, i.e., the ϵ, ζ, α, β, γ, and δ torsion angles (C3′-O3′-P-O5′-C5′-C4′-C3′). Theoretical calculations (Gorenstein, 1994; Giessner-Pettre et al., 1984; Gorenstein & Kar, 1975) suggest that ^{31}P chemical shifts are strongly dependent on the backbone torsion angles, in particular, α and ζ. These chemical-shift calculations and later empirical studies indicated that the ^{31}P resonance of a phosphate diester with a torsion angle α (or ζ) in a *t* (i.e., B_{II}) conformation should be several ppm downfield from the ^{31}P signal of an ester with its α (or ζ) torsion angle in a *g* (i.e., B_I) conformation. In the present structure, intercalation of the hydrocarbon between and parallel to adjacent base pairs (dG_{13}-dC_6 and dG_{14}-dA_5) has

Scheme 1

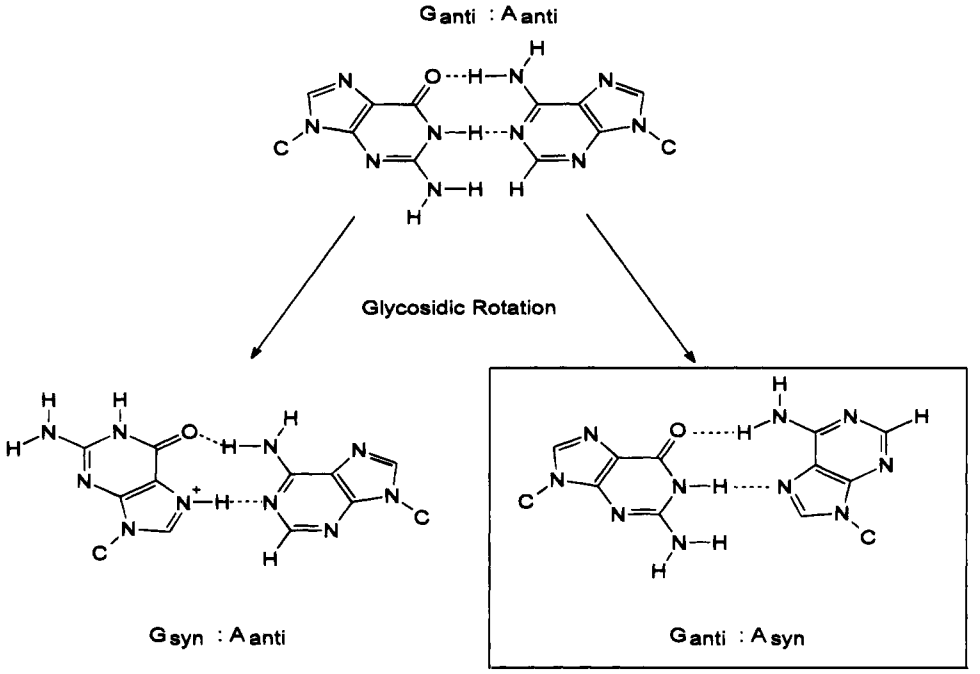

resulted in a widening of the distance between the two adjacent dG bases and a distortion of the sugar–phosphate backbone at the modified region. Some but not all of the rMD/energy minimized structures generated from NOE distance restraints exhibited atypical backbone torsion angles at the modified site. The observation of a downfield shift of ~2.5 ppm for the 14P (G_{13}-P-G_{14}) resonance and ~1.6 ppm for the 5P (C_4-P-A_5) resonance in comparison to the other phosphates is consistent with a B_{II} conformation for the phosphate diesters corresponding to 14P and 5P. Unusual torsional angles could also explain the unusual relative intensities in the $^{31}P-^{1}H$ correlation spectrum for the G_{13}-P-G_{14} phosphate. Backbone distortion has been noted in crystal structures as well as NMR structures of DNA–drug complexes (Searle, 1993). B_{II} phosphodiester conformations have also been observed in DNA containing dG-dA mismatch base pairs that use unusual hydrogen bonding partners (Chou et al., 1992a).

To date, we have been unsuccessful in obtaining interpretable NMR spectra from an oligonucleotide duplex with a complementary dT opposite dA modified at the exocyclic amino group by trans addition to (+)-BaP DE2, the most carcinogenic and hence arguably most biologically interesting of the four metabolically possible BaP 7,8-diol-9,10-epoxides. As previously noted, the 10*S*-[BaP]dA•dT 9-mer duplex, corresponding to the present structure but with a dT in place of the mispaired dG, has an unacceptably low T_m indicative of low thermal stability. Use of the same sequence extended by a 5′-terminal dC and a 3′-terminal dG in each strand provided a 10*S*-[BaP]dA•dT 11-mer duplex with a T_m of 35 °C. However, despite the increased stability of the duplex, its NMR spectrum indicated the presence of multiple conformations that interconvert slowly on the NMR time scale (Yeh et al., unpublished observations). The red-shift of the pyrene chromophore (at ca. 350 nm) was only 3 nm for the 10*S*-[BaP]dA•dT 11-mer upon duplex formation at low temperature as opposed to a red-shift of 6 nm for the 9-mer mismatch duplex of the present study. We speculate that this observation is related to the conformational heterogeneity of the 10*S*-[BaP]dA•dT 11-mer duplex, as seen in its NMR spectrum, and may reflect an equilibrium between intercalated and nonintercalated orientations of the hydrocarbon. We also speculate that a dG mismatch (as opposed to a dT match) opposite a 10*S*-dA adduct increases the thermal stability of the duplex and its preference for a single dominant conformation because of a preference of the 10*S*-dA adduct (but not the corresponding 10*R*-dA adduct) for a *syn* glycosidic torsional angle. Stabilization of this *syn* conformation by hydrogen bonding occurs with a mismatched dG but not a complementary dT residue. In contrast, the 10*R*-dA adduct prefers the *anti* conformation (Schurter et al., 1995a), so that a dG residue cannot hydrogen-bond with it, and thus does not increase the thermal stability of the mispaired duplex relative to that with a complementary dT. Preliminary NMR evidence (Liu et al., in preparation) suggests that an 11-mer duplex containing such a 10*R*-dA DE2 adduct opposite a dT is conformationally homogeneous and is consistent with hydrocarbon intercalation.

ACKNOWLEDGMENT

We are indebted to Dr. Ad Bax and Dr. Andy Wang for valuable discussions and for obtaining a 600 MHz NOESY spectrum. The contents of this publication do not necessarily reflect the views or policies of the Department of Health and Human Services, nor does mention of trade names, commercial products, or organizations imply endorsement by the U.S. Government.

SUPPORTING INFORMATION AVAILABLE

Expanded H1′ to H2′ and H2″ region of the PECOSY spectrum of the 10*S*-[BaP]dA•dG 9-mer duplex in D_2O (Figure S1) along with a list (Table S1) of the restraints used in the modeling calculations (11 pages). Ordering information is given on any current masthead page.

REFERENCES

Altieri, A. S., & Byrd, R. A. (1995) *J. Magn. Reson. Ser. B 107*, 260–266.

Bax, A., & Davis, D. G. (1985) *J. Magn. Reson. 65*, 355−360.
Bax, A., & Lerner, L. (1988) *J. Magn. Reson. 79*, 429−438.
Boelens, R., Scheek, R. M., Dijkstra, K., & Kaptein R. (1985) *J. Magn. Reson. 62*, 378−386.
Boelens, R., Koning, T. M. G., & Kaptein, R. (1988) *J. Mol. Struct. 173*, 299−311.
Boelens, R., Koning, T. M. G., van der Marcel, G. A., van Boom, J. H., & Kaptein, R. (1989) *J. Magn. Reson. 82*, 290−308.
Brown, T., Leonard, G. A., Booth, E. D., & Kneale, G. (1990) *J. Mol. Biol. 212*, 437−440.
Bullock, F. J., & Jardetzky, D. (1964) *J. Org. Chem. 29*, 1988−1990.
Cheng, S. C., Hilton, B. D., Roman, J. M., & Dipple, A. (1989) *Chem. Res. Toxicol. 2*, 334−340.
Chou, S. H., Cheng, J. W., Fedoroff, O. Y., Chuprina, V. P., & Reid, B. R. (1992a) *J. Am. Chem. Soc. 114*, 3114−3115.
Chou, S. H., Cheng, J. W., & Reid, B. R. (1992b) *J. Mol. Biol. 228*, 138−155.
Cosman, M., de los Santos, C., Fiala, R., Hingerty, B. E., Singh, S. B., Ibanez, V., Margulis, L. A., Live, D., Geacintov, N. E., Broyde, S., & Patel, D. J. (1992) *Proc. Natl. Acad. Sci. U.S.A. 89*, 1914−1918.
Cosman, M., de los Santos, C., Fiala, R., Hingerty, B. E., Ibanez, V., Luna, E., Harvey, R., Geacintov, N. E., Broyde, S., & Patel, D. J. (1993a) *Biochemistry 32*, 4145−4155.
Cosman, M., Fiala, R., Hingerty, B. E., Laryea, A., Lee, H., Harvey, R., Amin, S., Geacintov, N. E., Broyde, S., & Patel, D. J. (1993b) *Biochemistry 32*, 12488−12497.
Cosman, M., Fiala, R., Hingerty, B. E., Amin, S., Geacintov, N. E., Broyde, S., & Patel, D. J. (1994a) *Biochemistry 33*, 11507−11517.
Cosman, M., Fiala, R., Hingerty, B. E., Amin, S., Geacintov, N. E., Broyde, S., & Patel, D. J. (1994b) *Biochemistry 33*, 11518−11527.
Cosman, M., Laryea, A., Fiala, R., Hingerty, B. E., Amin, S., Geacintov, N. E., Broyde, S., & Patel, D. J. (1995) *Biochemistry 34*, 1295−1307.
de los Santos, C., Kouchakdjian, M., Yarema, K., Basu, A., Essigmann, J., & Patel, D. J. (1991) *Biochemistry 30*, 1828−1835.
de los Santos, C., Cosman, M., Hingerty, B. E., Ibanez, V., Margulis, L. A., Geacintov, N. E., Broyde, S., & Patel, D. J. (1992) *Biochemistry 31*, 5245−5252.
Gao, X., & Patel, D. J. (1988) *J. Am. Chem. Soc. 110*, 5178−5182.
Giessner-Pettre, C., Pullman, B., Prado, F. R., Cheng, D. M., Ivorno, V., & T'so, P. O. (1984) *Biopolymers 23*, 377−388.
Gonzalez, C., Rullmann, J. A. C., Bonvin, A. M. J. J., Boelens, R., & Kaptein, R. (1991) *J. Magn. Reson. 91*, 659−664.
Gorenstein, D. G. (1994) *Chem. Rev. 94*, 1315−1338.
Gorenstein, D. G., & Kar, D. (1975) *Biochem. Biophys. Res. Commun. 65*, 1073−1080.
Hare, D. R., Wemmer, D. E., Chou, S. H., Drobny, G., & Reid, B. R. (1983) *J. Mol. Biol. 171*, 319−336.
Hingerty, B. E., & Broyde, S. (1985) *Biopolymers 24*, 2279−2299.
Hore, P. J. (1983) *J. Magn. Reson. 55*, 283−300.
Hunter, W. N., Brown, T., & Kennard, O. J. (1986) *Biomol. Struct. Dyn. 4*, 173−191.
Jerina, D. M., & Daly, J. W. (1976) in *Drug Metabolism—from Microbe to Man* (Parke, D. V., & Smith, R. L., Eds.) pp 13−32, Taylor and Francis Ltd., London.
Jerina, D. M., Lehr, R. E., Yagi, H., Hernandez, O., Dansette, P. M., Wislocki, P. G., Wood, A. W., Chang, R. L., Levin, W., & Conney, A. H. (1976) in *In Vitro Metabolic Activation In Mutagenesis Testing* (de Serres, F. J., Fouts, J. R., Bend, J. R., & Philpot, R. M., Eds.) pp 159−177, Elsevier/North-Holland Biomedical Press, Amsterdam.
Jerina, D. M., Yagi, H., Thakker, D. R., Sayer, J. M., van Bladeren, P. J., Lehr, R. E., Whalen, D. L., Levin, W., Chang, R. L., Wood, A. W., & Conney, A. H. (1984) in *Foreign Compound Metabolism* (Caldwell, J., & Paulson, G. D., Eds.) pp 257−266, Taylor and Francis Ltd., London.
Jerina, D. M., Chadha, A., Cheh, A. M., Schurdak, M. E., Wood, A. W., & Sayer, J. M. (1991) in *Biological Reactive Intermediates IV. Molecular and Cellular Effects and Their Impact on Human Health (Adv. Exp. Med. Biol. 283)* (Witmer, C. M., Snyder, R., Jollow, D. J., Kalf, G. F., Kocsis, J. J., & Sipes, I. G., Eds.) pp 533−553 and references therein, Plenum Press, New York.
Lakshman, M. K., Sayer, J. M., Yagi, H., & Jerina, D. M. (1992) *J. Org. Chem. 57*, 4585−4590.
Leonard, G. A., Booth, E. D., & Brown, T. (1990) *Nucleic Acids Res. 18*, 5617−5623.
Li, Y., Zon, G., & Wilson, W. D. (1991) *Proc. Natl. Acad. Sci. U.S.A. 88*, 26−30.
Marion, D., Ikura, M., Tschudin, R., & Bax, A. (1989) *J. Magn. Reson. 85*, 393−399.
Meehan, T., & Straub, K. (1979) *Nature 277*, 410−412.
Müller, L. (1987) *J. Magn. Reson. 72*, 191−196.
Piotto, M., Saudek, V., & Sklenár, V. (1992) *J. Biomol. NMR 2*, 661−665.
Rinkel, L. J., & Altona, C. (1987) *J. Biomol. Struct. Dyn. 4*, 621−649.
Saenger, W. (1984) in *Principles of Nucleic Acid Structure*, pp 266−267, Springer, New York.
Schurter, E. J., Yeh, H. J. C., Sayer, J. M., Lakshman, M. K., Yagi, H., Jerina, D. M., & Gorenstein, D. G. (1995a) *Biochemistry 34*, 1364−1375.
Schurter, E. J., Sayer, J. M., Oh-hara, T., Yeh, H. J. C., Yagi, H., Luxon, B. A., Jerina, D. M., & Gorenstein, D. G. (1995b) *Biochemistry 34*, 9009−9020.
Searle, M. S. (1993) in *Progress in NMR Spectroscopy*, Vol. 25, pp 403−480, Pergamon Press, London.
Sklenár, V., Miyashiro, H., Zon, G., Miles, H. T., & Bax, A. (1986) *FEBS Lett. 208*, 94−98.
States, D. J., Haberkorn, R. A., & Ruben, D. J. (1982) *J. Magn. Reson. 48*, 286−292.
Thakker, D. R., Yagi, H., Levin, W., Wood, A. W., Conney, A. H., & Jerina, D. M. (1985) in *Bioactivation of Foreign Compounds* (Anders, M. W., Ed.) pp 177−242, Academic Press, New York.
Thakker, D. R., Levin, W., Wood, A. W., Conney, A. H., Yagi, H., & Jerina, D. M. (1988) in *Drug Stereochemistry—Analytical Methods and Pharmacology* (Wainer, I. W., & Drayer, D. E., Eds.) pp 271−296, Marcel Dekker, Inc., New York.
Tomasz, M., Olson, J., & Mercado, C. M. (1972) *Biochemistry 11*, 1235−1241.
Webster, G. D., Sanderson, M. R., Skelly, J. V., Neidle, S., Swann, P. F., Li, B. F., & Tickle, I. J. (1990) *Proc. Natl. Acad. Sci. U.S.A. 87*, 6693−6697.
Wei, S.-J. C., Chang, R. L., Wong, C.-Q., Bhachech, N., Cui, X. X., Hennig, E., Yagi, H., Sayer, J. M., Jerina, D. M., Preston, B. D., & Conney, A. H. (1991) *Proc. Natl. Acad. Sci. U.S.A. 88*, 11227−11230.
Wei, S.-J. C., Chang, R. L., Bhachech, N., Cui, X. X., Merkler, K. A., Wong, C.-Q., Henning, E., Yagi, H., Jerina, D. M., & Conney, A. H. (1993) *Cancer Res. 53*, 3294−3301.
Wei, S.-J. C., Chang, R. L., Henning, E., Cui, X. X., Merkler, K. A., Wong, C.-Q., Yagi, H., Jerina, D. M., & Conney, A. H. (1994) *Carcinogenesis 15*, 1729−1735.
Wüthrich, K. (1986) *NMR of Proteins and Nucleic Acids*, Wiley, New York.
Ya, N.-Q., Smirnov, S., Cosman, M., Bhanot, S., Ibanez, V., & Geacintov, N. E. (1994) in *Structural Biology: The State of the Art (Proceedings of the Eighth Conversation, Biomolecular Stereodynamics, Vol. 2), State University of New York, Albany, NY, 1993*, (Sarma, R. H., & Sarma, M. H., Eds.) pp 349−366, Adenine Press, Schenectady, NY.

BI950788B